EUROPEAN ORGANIZATION FOR NUCLEAR RESEARCH

CERN-EP/84-156
16 November 1984

THE "ROMAN POT" SPECTROMETER AND THE VERTEX DETECTOR OF EXPERIMENT UA4 AT THE CERN SPS COLLIDER

Amsterdam[1]-CERN[2]-Genoa[3]-Naples[4]-Pisa[5] Collaboration

R. Battiston[5*], A. Bechini[5], F. Bosi[5], M. Bozzo[3], P.L. Braccini[5*], J. Buskens[1], F. Carbonara[4], R. Carrara[5], R. Castaldi[5], U. Cazzola[5], F. Cervelli[5], G. Chiefari[4], E. Drago[4], R. Gorini[4], M. Haguenauer[2], B. Koene[1], R. Maleyran[2], F. Manna[4], G. Matthiae[4], L. Merola[4], A. Morelli[3], M. Napolitano[4], V. Palladino[1], P. Rewiersma[1], M. Robert[2], G. Roiron[2], G. Sanguinetti[5], H. Schuijlenburg[1], G. Sciacca[4], G. Sette[3], R. van Swol[1], J. Timmermans[1], L. Traspedini[3], C. Vannini[5], J. Velasco[2**] and F. Visco[4]

(Submitted to Nuclear Instruments and Methods)

---

1. NIKHEF-H, Amsterdam, The Netherlands.
2. CERN, Geneva, Switzerland.
3. Dipartimento di Fisica dell'Università e Sezione INFN, Genoa, Italy.
4. Dipartimento di Fisica dell'Università e Sezione INFN, Naples, Italy.
5. Dipartimento di Fisica dell'Università e Sezione INFN, Pisa, Italy.
* Also at University of Perugia, Italy.
** Permanent address: IFIC, University of Valencia, Spain.

ABSTRACT

We describe the apparatus used by experiment UA4 to study proton-antiproton elastic and inelastic interactions at the CERN SPS Collider. Elastically scattered particles, travelling at very small angles, are observed by detectors placed inside movable sections ("Roman pots") of the SPS vacuum chamber. The deflection in the field of the machine quadrupoles allows the measurement of the particle momentum. Inelastic interactions are observed by a left-right symmetric system of trigger counter hodoscopes and drift-chamber telescopes. The apparatus reconstructs the interaction vertex and measures the pseudorapidity η of charged particles in the range $2.5 < |\eta| < 5.6$.

1. INTRODUCTION

Experiment UA4 was specifically designed to measure the total cross-section and elastic scattering at the CERN $p\bar{p}$ Collider. The total cross-section was obtained from the measurement of elastic scattering at low momentum transfer and of the inelastic interaction rate, making use of the optical theorem [1,2]. This method, already used at the ISR [3], does not require an independent determination of the machine luminosity.

The UA4 experimental apparatus, located in the long straight section LSS4 at the CERN SPS, is symmetric with respect to the crossing point and consists of two different sets of detectors, one set for elastic scattering and one for inelastic interactions.

The study of elastic scattering at the Collider (centre-of-mass energy $\sqrt{s}$ = 546 GeV) requires detection of particles emitted at angles of the order of 1 mrad with respect to the circulating beams. This is achieved by placing the detectors inside movable sections of the vacuum chamber ("Roman pots"), which are moved vertically toward the beam plane once stable beam conditions are reached. This technique was already employed at the ISR [4]. The elastic detector is able to measure, together with the direction of the scattered particles, also their momentum, by taking advantage of the deflection of the trajectories in the magnetic field of the machine quadrupoles. This feature was useful to reject background in large-$|t|$ elastic scattering [5]. In addition, it allowed the study of inelastic diffractive scattering [6] by measuring the momentum spectrum of particles emitted at small angles.

The measurement of the inelastic rate requires a large-coverage system satisfying two basic requirements: maximum inclusiveness and clear discrimination of beam-beam events from background. The inelastic detector covers the pseudorapidity region $2.5 < |\eta| < 5.6$ on both sides of the inter-

action point. Owing to the high average multiplicity and broad rapidity distribution of the charged secondaries, this angular coverage detects about 99% of the total inelastic rate. The central detector of experiment UA2 [7] (installed in LSS4 and covering the large-angle region, $|\eta| < 1.7$) was used to detect interactions with charged-particle production at large angles only and to study special classes of events.

The discrimination of beam-beam interactions from background is obtained by use of time-of-flight information and by reconstructing an interaction vertex from the observed tracks.

2. THE ELASTIC SCATTERING DETECTOR

2.1 The layout

One arm of the apparatus is shown schematically in fig. 1. The detectors, located inside sixteen pots, are arranged in eight telescopes of two pots each, placed symmetrically on the left and the right side of the interaction point, above and below the machine plane. The four inner telescopes P_1 are at a distance of about 22 m from the crossing point and are located between two machine quadrupoles Q_1 and Q_2; the four outer telescopes P_2 are at a distance of about 37 m. The two pots of the inner telescopes are 3 m apart, while those of the outer telescopes are about 6 m apart. This difference is due to the available space.

2.2 The "Roman pots"

The mechanical construction of a pair of pots, one above and one below the machine plane, is sketched in fig. 2a. The two pots can be displaced along the same vertical axis. Each pot is cylindrical in shape with 0.1 mm thick steel windows (6 cm wide, 12 cm high) on the front and back side for the passage of particles. The edge of the pot has a circular

flange, which is connected to the vacuum chamber of the machine by bellows of 30 cm in diameter. The atmospheric pressure on the pot is balanced by a specially designed pneumatic system; as a consequence the pots can easily be displaced by means of low-power electric motors. The vertical position of the pots is monitored by linear transducers of uniform resistivity with an accuracy better than 50 μm. The absolute position of the pots with respect to the machine axis was repeatedly measured by the survey group of the SPS with a precision better than 100 μm. The vertical alignment of the pots was also checked to the same accuracy by means of a hydrostatic system.

2.3 The chambers and counters

A wire chamber, a hodoscope of vertical ("finger") scintillation counters, and a trigger counter were placed inside each pot. They are shown in fig. 2b. In order to detect particles scattered at very small angles, the sensitive area of the chambers must be as close as possible to the machine plane. Therefore, the mechanical support of the chambers is U-shaped, with a thin wall on the side facing the beam, and the sensitive area of the chambers starts already a few tenths of a millimetre from the bottom of the pot.

The vertical track coordinate is measured by four drift planes with horizontal wires. Each drift plane contains three drift cells of conventional geometry, which are suitably staggered to resolve the up-down ambiguity and to allow a self-calibration of the drift velocity and of the time zero offset of the drift-time measurements. The single-plane drift resolution, as determined from the track reconstruction during data taking, was about 130 μm, providing a measurement of the track position in the vertical plane with a r.m.s. error of about 70 μm. In the wire chamber the four drift planes are followed by a proportional plane with horizontal

wires of high resistivity. The horizontal track coordinate is measured with an accuracy of about 400 μm, by using the charge-division method on these wires. More details on the construction and operation of these chambers are given elsewhere [8] .

The hodoscope of eight vertical finger counters is followed by a trigger counter, 45 mm wide, 110 mm high, covering the active region of the chamber. The trigger counter is viewed through two independent light-guides by two photomultipliers to provide a uniform response. The efficiency of the trigger counters was continuously monitored by measuring their pulse height. The finger counters provide the absolute calibration for the charge-division measurement of the wire chambers.

3. THE INELASTIC DETECTOR

3.1 The layout

The apparatus to measure the inelastic rate is shown in fig. 3. Two identical systems of three telescopes (D_1, D_2, D_3) placed symmetrically on the left and right sides of the crossing region cover polar angles from 0.4° up to 10°, corresponding to the pseudorapidity range $2.5 < |\eta| < 5.6$. Each telescope is composed of six drift chamber planes followed by a plane of trigger counters (T_1, T_2 and T_3, respectively). The coordinate along the drift wire is measured by means of a delay line close to the drift wire itself, which provides an unambiguous reconstruction of space points. The track-finding procedure is therefore greatly simplified. Moreover the readout of the delay line at both ends provides a constraint that facilitates handling multiple hits.

Telescope D_1 is 40 cm long and is placed at ~ 1.5 m from the interaction point, covering the range $2.5 < |\eta| < 3.2$. It is made of 24 drift chamber modules assembled inside 4 independent plexiglas boxes, with 6 planes each.

Telescope D_2, which is 1.5 m long, is placed at ~ 4.5 m from the interaction point and covers the pseudorapidity interval $3.0 < |\eta| < 4.8$, partially overlapping with D_1. It is made of 12 L-shaped chambers assembled in two sets of 6 chambers each. Telescope D_3 is at ~ 10 m from the interaction point and covers the range $4.4 < |\eta| < 5.6$, i.e. the angular region below 1.5°. It is made of the same chamber modules as telescope D_1. The six planes of this small-angle telescope are distributed over a longer distance (3.5 m) to keep the same lever arm as the other telescopes.

Between the crossing point of the beams and D_2, the vacuum chamber is a corrugated stainless-steel pipe, 16 cm in diameter and 0.15 mm thick. In front of D_3, it consists of a stainless-steel cylinder 60 cm in diameter; particles emitted at angles below 1.5° traverse only the 0.5 mm thick window of this cylinder before reaching D_3.

The region of polar angles $\theta > 20°$ ($|\eta| < 1.7$) is covered by the central detector (CD) of the UA2 Collaboration [7] that was also used in the data taking. All detectors have full azimuthal acceptance and together they provide complete solid-angle coverage around the crossing region, with the exception of a small gap for θ between 10° and 20° and of the forward region, $\theta < 0.4°$, which is made inaccessible by the presence of the vacuum pipe.

Two symmetrical telescopes of three scintillation counters each, placed at a distance of ~ 11 m from the crossing point on both sides, viewed the interaction region under an angle of ~ 5°. The left-right coincidence of these counters is affected by negligible background (< 0.1%) and provides a luminosity monitor which detects about 6.2% of the total inelastic rate.

3.2 The chambers and counters

Telescopes D_1 and D_3 are made of small drift-chamber modules having different lengths along the sense wires (between 31 and 38 cm) but the same cross-sectional structure. The drift regions are bounded by a pair of epoxy fibre-glass printed-circuit boards. The usual field-shaping wires are replaced by cathode strips printed on the circuit boards. There are four drift cells in each module with two pairs of 20 μm gold-plated tungsten wires in between the circuit boards. The spacing between a pair of sense wires is 1.8 mm so as to avoid left-right ambiguity. Each drift cell has a depth of 11 mm and a drift space of 41 mm. Parallel to the wires, a cylindrical delay line of 3.2 mm diameter measures the coordinate along the sense wire. The specific delay is 7.4 ns/cm and the characteristic impedance is 1200 Ω.

The L-shaped D_2 chambers have the wires parallel to their longest side ($\sim$ 1 m). Two of these chambers together form a 1 m x 1 m sensitive area around the beam pipe. The spacing between the 20 μm gold-plated tungsten sense wires is 54 mm. The field-shaping, as in the case of D_1 and D_3, is obtained by cathode strips printed on circuit boards. Each chamber contains two planes of staggered parallel wires to solve left-right ambiguity: one of them is equipped with flat delay lines, facing the sense wires, which have a cross-section 2.1 x 4.2 mm^2. The specific delay of these lines is 5.2 ns/cm and their characteristic impedance is 680 Ω.

More details about the construction and performance of these chambers can be found in ref. [9] for D_1 and D_3 and in ref. [10] for D_2.

The intrinsic drift coordinate resolution has been measured to be better than 200 μm for all chambers, including the calibration uncertainties. From track fitting on data, the actual resolution on the drift and on delay-line coordinates are found to be 340 μm and 2.1 mm, respectively, for D_1 and

D_3. For the telescope D_2 the corresponding figures are 600 μm and 2.8 mm. These values of the resolution include alignment errors of the different modules inside each telescope.

4. TRIGGER ELECTRONICS AND DATA ACQUISITION

The elastic trigger consisted of the logical OR of two left-right coincidences (up-left x down-right + down-left x up-right) of the trigger counters of telescopes on the two sides of the crossing region. The fraction of good elastic events was approximately 50% for low-|t| measurements ($-t < 0.5$ GeV^2). The trigger for measurements at larger |t| ($-t > 0.5$ GeV^2) had to be made more selective by requiring no simultaneous hits on both up and down counters on the same side. "Splashes" of secondary particles generated in the vacuum chamber by inelastic interactions or halo particles were so rejected. The fraction of the good events never went below 30% of the triggers recorded on tape.

The measurement of the total inelastic rate requires a trigger as inclusive as possible and a clear discrimination of beam-beam events from background interactions. The following triggers were used:

- A double-arm trigger $[(T_2 + T_3)_{left} \times (T_2 + T_3)_{right}]$ covering the range $3.0 < |\eta| < 5.6$ on each side, which detects almost the totality of non-diffractive events.
- A single-arm trigger $[(T_1 + T_2 + T_3)_{left} \times \overline{(T_2 + T_3)}_{right}]$ covering the range $2.5 < \eta < 5.6$ on the outgoing $\bar{p}$ side. It detects events escaping the double-arm trigger, mostly diffractive interactions with all visible tracks in one arm only.
- A central-detector trigger $[CD \times \overline{(T_2 + T_3)}_{left+right}]$ which detects events with charged particles at large angles only, in the range $-1.7 < \eta < 1.7$.

The relative contributions of these triggers to the total inelastic rate were found to be 82.7%, 16.3%, and 0.1%, respectively [2]: the remaining ~ 1%, due to the losses in the beam pipe or in the gap between D_1 and the central detector, was estimated by extrapolation.

Other triggers were also used to study particular types of events. For diffractive events, a trigger requiring the coincidence of the elastic telescopes on one side with the inelastic counters on the other side of the crossing point was used [6] .

Data acquisition was performed via an enhanced performance CAMAC-like system (REMUS). The bulk of the data consisted of the time digitization from drift wires and delay lines. A time-to-digital converter system having 1.5 ns time bin and a multi-hit capability of up to fourteen different time measurements per channel was used [11] . The signals at both ends of each charge-division wire, amplified by charge-integrating amplifiers, were digitized by peak-sensing analog-to-digital converters.

All trigger signals were timed with respect to a gate signal synchronous with the bunch crossing in the interaction region. With three proton and three antiproton bunches circulating in the machine, there was a crossing every 7.7 μs. The gate signal was used to start the conversion process of all ADC and TDC channels at each bunch crossing. If no trigger was detected, the conversion was stopped and all the electronics was reset about 2 μs after the crossing. When a trigger signal was present (the trigger-forming time was about 400 ns) the conversion process continued, a busy signal was generated, and an interrupt was sent to the on-line computer for data acquisition.

5. OPERATION AND PERFORMANCE OF THE SYSTEM

5.1 Elastic scattering

In the present experiment elastically or quasi-elastically scattered particles are detected after traversing the machine quadrupoles Q_1 and Q_2. Therefore, the operation of the system is closely related to the optics of the machine in the intersection region which is determined by the strength of the machine quadrupoles. The optics is defined by the values of the betatron function at the crossing point in the horizontal and vertical planes, β_H and β_V. The beam emittance ε and the betatron function determine the size σ and the angular spread σ' of the beam at the crossing point. Their r.m.s. values are given by $\sigma = (1/2)(\varepsilon\beta)^{1/2}$ and $\sigma' = (1/2)(\varepsilon/\beta)^{1/2}$ in either the horizontal or the vertical plane. For a given emittance and a given number of circulating particles the luminosity depends on the β-function as $(\beta_H\beta_V)^{-1/2}$. Data were taken using different machine optics whose parameters are collected in table 1: the values of σ_V and σ'_V correspond to a vertical beam emittance ε = 0.08 mm mrad. The horizontal beam emittance is similar to the vertical one, so beam size and angular spread in the horizontal plane are similar to those given in table 1 for the vertical plane.

The minimum accessible scattering angle is determined by the smallest distance of approach of the pots to the beam, which depends on the machine optics. It was empirically found that a reasonable setting of the pots corresponds to a distance of the edge of the sensitive region of the detectors from the beam equal to about fifteen times the r.m.s. size of the beam at the position of the pot itself. Typical distance from the edge of the sensitive region of the chamber to the beam axis was 15-25 mm, depending on the optics and the pot position. Single rates for good, not noisy,

stacks were a few hundred Hz, while the noise current drawn by the drift planes of each chamber was less than 1 μA.

The maximum accessible value of the scattering angle is determined by the aperture of the vacuum chamber. By increasing the strength of the quadrupoles Q_1 and Q_2, the betatron function at the crossing decreases. As a consequence, scattered particles become more strongly focused toward the machine plane (fig. 4) and the accepted interval of scattering angles moves upwards. The maximum value of $|t|$ is limited to $-t = 1.6\ GeV^2$ in low-β optics by the aperture of the vacuum chamber inside the quadrupoles Q_1. From the study of different optics it is clear that it is not always possible to make use of all pot telescopes. This could be done for the "squeezed-β" optics, while in the "high-β" mode only the outer telescopes P_2 were used and in the "medium-β" mode [12] only the inner ones P_1. The low-β optics is not quite symmetric and P_2 telescopes on the right side could not be used.

Particle deflection through the quadrupoles was calculated with the standard formalism of transfer matrices using the strength and the effective length of the quadrupoles which are known in absolute value with an accuracy of better than 3×10^{-3}. For all the different optics the quadrupole pair Q_1 is focusing in the vertical plane, while the pair Q_2 is defocusing. Trajectories for elastic scattering in the vertical plane corresponding to different optics are shown in fig. 4.

If the detector resolution is sufficiently good, the uncertainty on the measured scattering angle θ is determined by the angular spread of the beam in the vertical plane as $\Delta\theta \simeq (1/\sqrt{2})\sigma'_V$. The actual angular resolution $\Delta\theta$ is in fact obtained from the widths of the observed collinearity distributions $\theta(\bar{p}) - \theta(p)$ in both the vertical and the horizontal plane. An example of these distributions, as measured during the high-β runs, is

shown in fig. 5. For this optics the detector resolution and multiple scattering in the pots contribute, together with the beam angular spread, to the observed angular resolution. For the low-β optics, on the other hand, the angular spread of the beams represents the dominant contribution. Information on the resolution, which for a given optics is proportional to $(-t)^{1/2}$, is also collected in table 1.

As already noticed, our system of "Roman pots" is in fact a small-angle spectrometer able to measure flight direction and momentum of the scattered particles. The particle momentum is measured from the observed deflection of the trajectories by the magnetic field of the machine quadrupoles. In the low-β (and also squeezed-β) optics, particles having the same momentum p_0 as the beam are deflected in the vertical plane by the quadrupole pair Q_1 toward the machine axis by an angle which is about equal to $2\theta_V$, where θ_V is the vertical component of the production angle (fig. 4). The deflection by the quadrupole pair Q_2 is outward from the machine plane by an amount about equal to θ_V. The actual particle momentum p is obtained from the measured displacement of the trajectory in the vertical plane at the four pots of the two telescopes P_1 and P_2, using in addition the constraint of the vertex position. The momentum resolution of the system was evaluated by analysing elastic scattering events which were identified on the basis of the collinearity requirement. For the low-β optics the observed momentum resolution has an r.m.s. value of 0.6% (fig. 6a) which is determined by the measurement errors, the intrinsic momentum spread of the beam being only a few times 10^{-4}. This momentum resolution is quite useful to clean the sample of elastic event candidates at large $|t|$, by rejecting the background of inelastic interactions. In addition, it allowed a measurement [6] of the momentum spectrum of inelastically scattered antiproton in the reaction $\bar{p}p \to \bar{p}X$. For the high-β optics the observed momentum

resolution, as shown in fig. 6b, is much poorer: it is about 8%. This is due to the much smaller deflection angle of the quadrupoles (fig. 4) and to the fact that the tracks are measured only by the two pots of the outer telescopes P_2.

5.2 Inelastic interactions

In order to discriminate beam-beam interactions from background, the first step of the analysis is based on a check of the time-of-flight configuration of the trigger counters T_1, T_2, and T_3. Figures 7a, 7b, and 7c show two well-separated peaks: the one on the left corresponds to halo particles in time with the incoming beam ("in"), while the peak on the right is due to outgoing particles. A selection is made by rejecting the events affected by "in" hits: about 50% of the triggers of the high-β runs are so removed. In the low-β runs only a few per cent of triggers have a bad time-of-flight configuration since the background rate remains almost constant, while the much higher luminosity increases the rate of good events. In the surviving triggers, beam-beam interactions are recognized by demanding a vertex from the tracks fitted to the space points in the drift chambers D_1, D_2, and D_3.

A particle which hits a chamber generates three signals, one on the sense wire and one on each of the two extremities of the delay line. The readout of the delay line at both ends provides a constraint that facilitates the handling of multiple hits, since the timings t_{d1} and t_{d2} of these two signals and the drift time t_{sw} are bound by the following relation:

$$\tau = t_{d1} + t_{d2} - 2t_{sw} - T = 0 \ ,$$

where the constant T is the transit time in the delay line. The distribution of the variable τ is shown in fig. 8a, where the high signal-to-

background ratio indicates that the reconstruction of the space points is done with almost no ambiguity.

Tracks are reconstructed by demanding track points in at least four of six drift chamber planes in any telescope. This requirement ensures full detection efficiency for charged particles over the entire solid angle covered by the apparatus. The errors on the space points were evaluated in actual running conditions, from the observed distributions of the fit residuals (figs. 8b and 8c). For each fitted track,the full covariance matrix was then computed. The search for an interaction vertex was performed by means of a clustering algorithm which retained only the tracks contributing an amount smaller than three standard deviations to the total X^2 of the vertex. The transverse distribution of the reconstructed vertices is plotted in fig. 9a. Its width (~ 7 mm), although larger than the transverse-beam dimensions, allows the rejection of all beam-pipe interactions. The longitudinal distributions of the reconstructed vertices for both double- and single-arm triggers are shown in figs. 9b and 9c, respectively. The tails in fig. 9c are larger than those in fig. 9b because the lower multiplicity and the smaller average angles of tracks in the single-arm events increase the error of the z-coordinate of the vertex.

6. CONCLUSION

The present set-up has been running satisfactorily during the first three years of operation of the SPS Collider (1981-1983). It proved to be very suitable for measuring the total cross-section, elastic scattering, and diffractive dissociation. It will be ready to measure in 1985, with minor changes, the ratio between the real and the imaginary part of the forward elastic scattering amplitude using the classical method of Coulomb interference [13] .

Acknowledgements

The authors wish to thank the staff of the CERN SPS Division for their help in the installation and survey of the apparatus. The effort of many technicians at CERN, INFN, and NIKHEF who contributed to the design, construction, and installation of the apparatus is warmly acknowledged; we particularly wish to thank L. Corucci, M. Del Colletto, G. Favati, M. Favati, M. Givoletti, J.L. Loquet, F. Malvano, G. Manto and C. Tornatore. Special thanks are due to D. Passuello and P. Salvadori for the setting up and running of the TDC system.

REFERENCES

[1] R. Battiston, M. Bozzo, P.L. Braccini, F. Carbonara, R. Carrara, R. Castaldi, F. Cervelli, G. Chiefari, E. Drago, M. Haguenauer, B. Koene, L. Linssen, G. Matthiae, L. Merola, M. Napolitano, V. Palladino, G. Sanguinetti, G. Sciacca, G. Sette, R. van Swol, J. Timmermans, C. Vannini, J. Velasco and F. Visco, Phys. Lett. 115B (1982) 333.

R. Battiston, M. Bozzo, P.L. Braccini, F. Carbonara, R. Carrara, R. Castaldi, F. Cervelli, G. Chiefari, E. Drago, M. Haguenauer, B. Koene, G. Matthiae, L. Merola, M. Napolitano, V. Palladino, G. Sanguinetti, G. Sciacca, G. Sette, R. van Swol, J. Timmermans, C. Vannini, J. Velasco and F. Visco, Phys. Lett. 117B (1982) 126.

[2] M. Bozzo, P.L. Braccini, F. Carbonara, R. Castaldi, F. Cervelli, G. Chiefari, E. Drago, M. Haguenauer, V. Innocente, B. Koene, S. Lanzano, G. Matthiae, L. Merola, M. Napolitano, V. Palladino, G. Sanguinetti, S. Scapellato, G. Sciacca, G. Sette, R. van Swol, J. Timmermans, C. Vannini, J. Velasco and F. Visco, Phys. Lett. 147B (1984) 385.

M. Bozzo, P.L. Braccini, F. Carbonara, R. Castaldi, F. Cervelli, G. Chiefari, E. Drago, M. Haguenauer, V. Innocente, B. Koene, S. Lanzano, G. Matthiae, L. Merola, M. Napolitano, V. Palladino, G. Sanguinetti, S. Scapellato, G. Sciacca, G. Sette, R. van Swol, J. Timmermans, C. Vannini, J. Velasco and F. Visco, Phys. Lett. 147B (1984) 392.

[3] U. Amaldi, G. Cocconi, A.N. Diddens, Z. Dimčovski, R.W. Dobinson, J. Dorenbosch, P. Duinker, G. Matthiae, A.M. Thorndike, A.M. Wetherell, G. Bellettini, P. L. Braccini, R. Castaldi, V. Cavasinni, T. Del Prete, P. Laurelli, M.M. Massai, M. Morganti, G. Sanguinetti, M. Valdata-Nappi, A. Baroncelli, C. Bosio, G. Abshire, J. Crouch, G. Finocchiaro, P. Grannis, H. Jöstlein, R. Kephart, D. Lloyd-Owen and R. Thun, Phys. Lett. 62B (1976) 460.

U. Amaldi, G. Cocconi, A.N. Diddens, Z. Dimčovski, R. W. Dobinson, J. Dorenbosch, P. Duinker, G. Matthiae, A.M. Thorndike, A.M. Wetherell, G. Bellettini, P.L. Braccini, R. Carrara, R. Castaldi, V. Cavasinni, F. Cervelli, T. Del Prete, P. Laurelli, M.M. Massai, M. Morganti, G. Sanguinetti, M. Valdata-Nappi, C. Vannini, A. Baroncelli, C. Bosio, G. Abshire, J. Crouch, G. Finocchiaro, P. Grannis, H. Jöstlein, R. Kephart, D. Lloyd-Owen and R. Thun, Nucl. Phys. B145 (1978) 367.

[4] U. Amaldi, R. Biancastelli, C. Bosio, G. Matthiae, J.V. Allaby, W. Bartel, M.M. Block, G. Cocconi, A.N. Diddens, R.W. Dobinson, J. Litt and A.M. Wetherell, Phys. Lett. 43B (1973) 231.

[5] M. Bozzo, P.L. Braccini, F. Carbonara, R. Carrara, R. Castaldi, F. Cervelli, G. Chiefari, E. Drago, M. Haguenauer, B. Koene, G. Matthiae, L. Merola, M. Napolitano, V. Palladino, G. Sanguinetti, G. Sciacca, G. Sette, R. van Swol, J. Timmermans, C. Vannini, J. Velasco and F. Visco, Contribution to the Int. Conf. on High Energy Physics, Brighton (UK), 1983, paper 0116.

[6] M. Bozzo, P.L. Braccini, F. Carbonara, R. Carrara, R. Castaldi, F. Cervelli, G. Chiefari, E. Drago, M. Haguenauer, B. Koene, G. Matthiae, L. Merola, M. Napolitano, V. Palladino, G. Sanguinetti, G. Sciacca, G. Sette, R. van Swol, J. Timmermans, C. Vannini, J. Velasco and F. Visco, Phys. Lett. 136B (1984) 217.

[7] M. Dialinas, J. Forget, D. Geoffroy, P. Jean and M. Vergand, Orsay report LAL-RT/83-14 (1983).

The UA2 Collaboration, presented by B. Mansoulié, Proc. 3rd Moriond Workshop on Antiproton-Proton Physics and the W Discovery, La Plagne, Savoie, 1983 (Ed. Frontières, Gif-sur-Yvette, 1983), p. 609.

[8] J. Buskens, B. Koene, L. Linssen, P. Rewiersma, H. Schuijlenburg, R. van Swol, J. Timmermans, M. Haguenauer, G. Roiron and J. Velasco, Nucl. Instrum. Methods 207 (1983) 365.

[9] A. Bechini, C. Betti, F. Bosi, P. L. Braccini, R. Carrara, R. Castaldi, V. Cavasinni, F. Cervelli, G. Ciancaglini, T. Del Prete, P. Laurelli, P. Marchi, M. Massai, M. Morganti, G. Sanguinetti, M. Valdata-Nappi and C. Vannini, Nucl. Instrum. Methods 156 (1978) 181.

[10] F. Carbonara, G. Chiefari, E. Drago, L. Merola, M. Napolitano, R. Rinzivillo, G. Sciacca and F. Visco, Nucl. Instrum. Methods 171 (1980) 479.

[11] F.W. Sippach, Columbia University, Nevis Lab., Irvington, New York (unpublished report).

[12] R. Battiston, M. Bozzo, P.L. Braccini, F. Carbonara, R. Carrara, R. Castaldi, F. Cervelli, G. Chiefari, E. Drago, M. Haguenauer, B. Koene, G. Matthiae, L. Merola, M. Napolitano, V. Palladino, G. Sanguinetti, G. Sciacca, G. Sette, R. van Swol, J. Timmermans, C. Vannini, J. Velasco and F. Visco, Phys. Lett. 127B (1983) 472.

[13] UA4 Collaboration, CERN/SPSC/84-7, SPSC/P 114/Add.3, 6 January 1984.

Table 1

Parameters of the different running conditions

Machine optics	High-β	Medium-β	Low-β	Squeezed-β
$\beta_H \times \beta_V$ (m x m)	100 x 100	7 x 3.5	2 x 1	1.3 x 0.65
σ_V (mm)	1.4	0.26	0.14	0.11
σ'_V (mrad)	0.014	0.076	0.14	0.18
Typical luminosity ($cm^{-2} s^{-1}$)	4×10^{26}	1.5×10^{27}	$(2\text{-}5) \times 10^{28}$	8×10^{28}
$\|t\|$-range (GeV^2)	0.03-0.35	0.21-0.50	0.4-1.5	0.6-1.6
θ resolution (mrad) intrinsic observed	 0.010 0.012	 0.054 0.060	 0.10 0.105	 0.12 0.12
t-resolution (GeV^2)	$0.006\sqrt{\|t\|}$	$0.032\sqrt{\|t\|}$	$0.057\sqrt{\|t\|}$	$0.065\sqrt{\|t\|}$
Pot telescopes used	P_2 left P_2 right	P_1 left P_2 right	$P_1 + P_2$ left P_2 right	$P_1 + P_2$ left $P_1 + P_2$ right
Momentum resolution (r.m.s. value)	8%		0.6%	

Figure captions

Fig. 1 : Layout of the "Roman pot" spectrometer. Only the left ($\bar{p}$) side is shown, the other side is symmetric with respect to the interaction point. Q_1 and Q_2 represent two pairs of machine quadrupoles. The detectors are placed inside the pots, arranged in telescopes P_1 and P_2.

Fig. 2 : a) Sketch of the mechanical structure holding two pots. A small section of the machine pipe is shown together with the bellows of the pot.

b) A detail of the detector is shown inside the pot (wire chamber, finger counters, and trigger counter) together with a perspective view.

Fig. 3 : Layout of one arm of the vertex detector (the full detector is symmetric with respect to the crossing region). The central detector of experiment UA2 is also sketched. The η acceptance of the trigger hodoscopes is indicated. One arm of the monitor telescopes is also shown.

Fig. 4 : Trajectories in the vertical plane for different optics. The squeezed-β optics is very similar to the low-β kind. The position of the pots is also shown.

Fig. 5 : Collinearity plots for (a) the vertical and (b) the horizontal plane obtained in the high-β runs. The offset in the horizontal collinearity distribution is due to the displacement of the beam in this plane.

Fig. 6 : Momentum resolution (a) for low-β and (b) for high-β optics, as determined from the analysis of elastic-scattering events: p is the measured momentum and p_0 is the beam momentum.

Fig. 7 : Time-of-flight spectra of trigger counters: (a) T_1, (b) T_2, and (c) T_3. The peak at the left is due to the incoming beam halo.

Fig.8 : a) Distribution of the quantity $\tau = t_{d1} + t_{d2} - 2t_{sw} - T$, where t_{sw}, t_{d1}, t_{d2} are the time readouts on the sense wire and on the two ends of the delay line and T is the transit time in the delay line.

b) Distribution of the track-fitting residuals in the drift coordinate.

c) Distribution of the track-fitting residuals in the delay-line coordinate.

Fig.9 : a) Transverse distribution of reconstructed vertices in double-arm events: the arrows indicate the position of the pipe wall.

b) Longitudinal distribution of vertices in double-arm events.

c) Longitudinal distribution of vertices in single-arm events.

ELASTIC SCATTERING LAYOUT

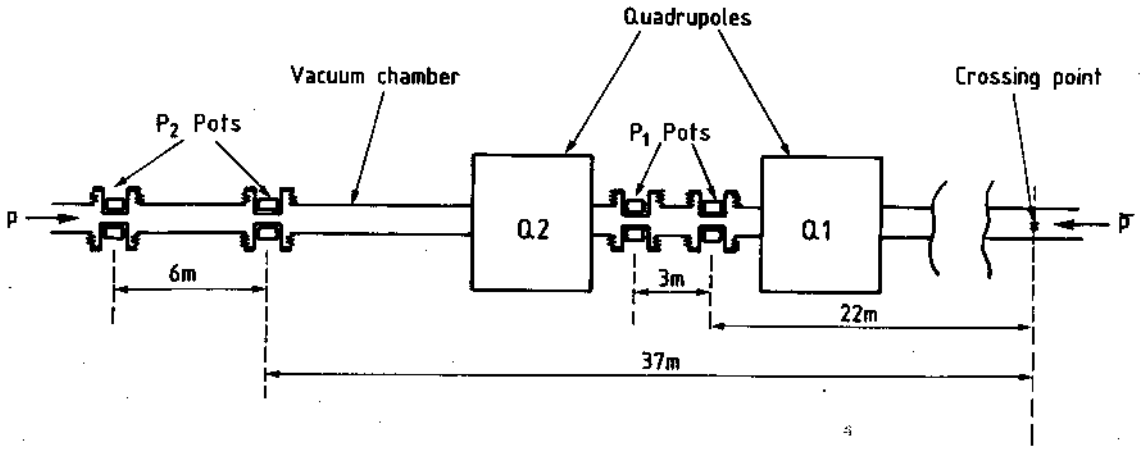

Fig. 1

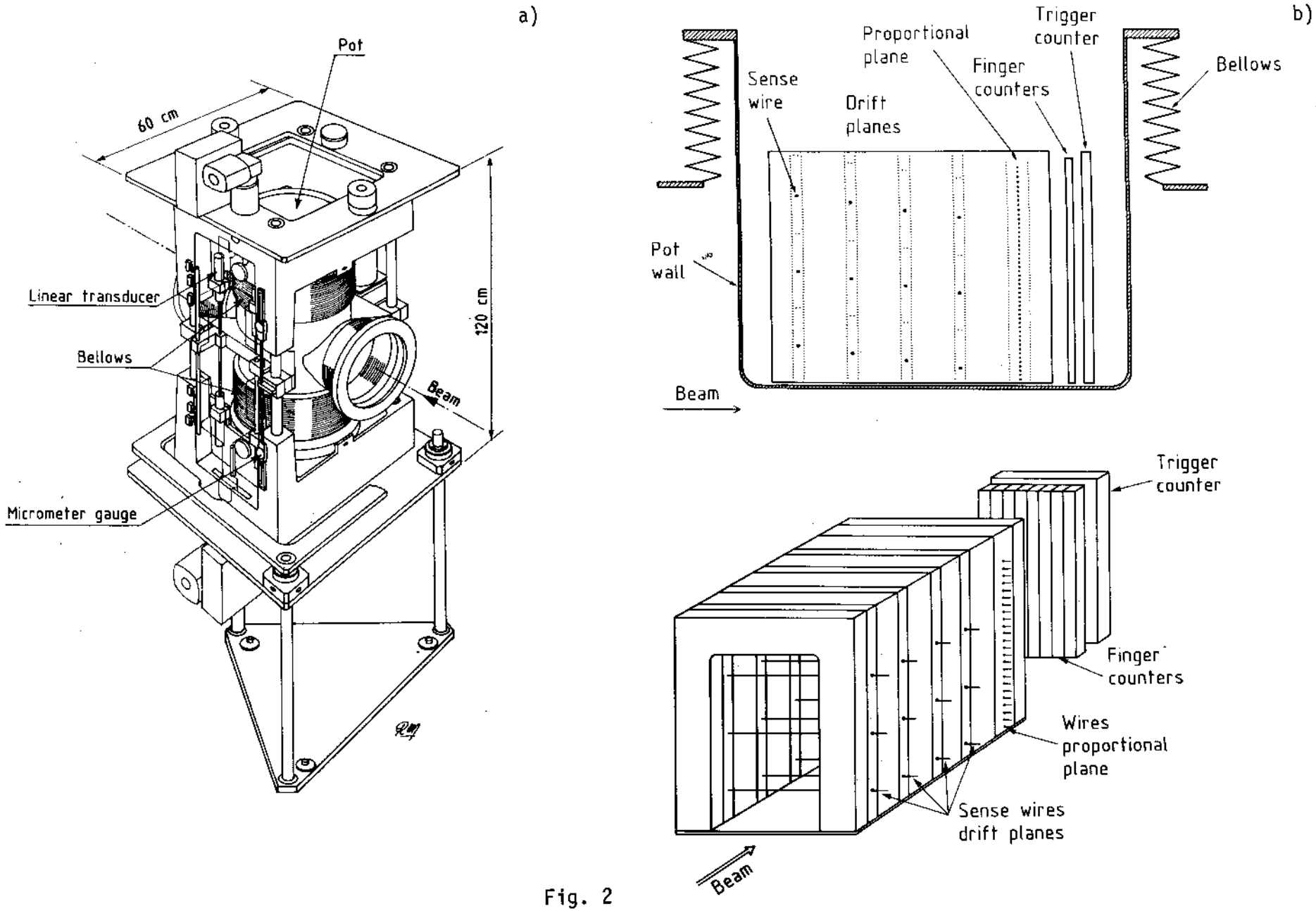
a)
Pot
60 cm
120 cm
Linear transducer
Bellows
Beam
Micrometer gauge
b)
Proportional plane
Trigger counter
Sense wire
Finger counters
Bellows
Drift planes
Pot wall
Beam
Trigger counter
Finger counters
Wires proportional plane
Sense wires drift planes
Beam

Fig. 2

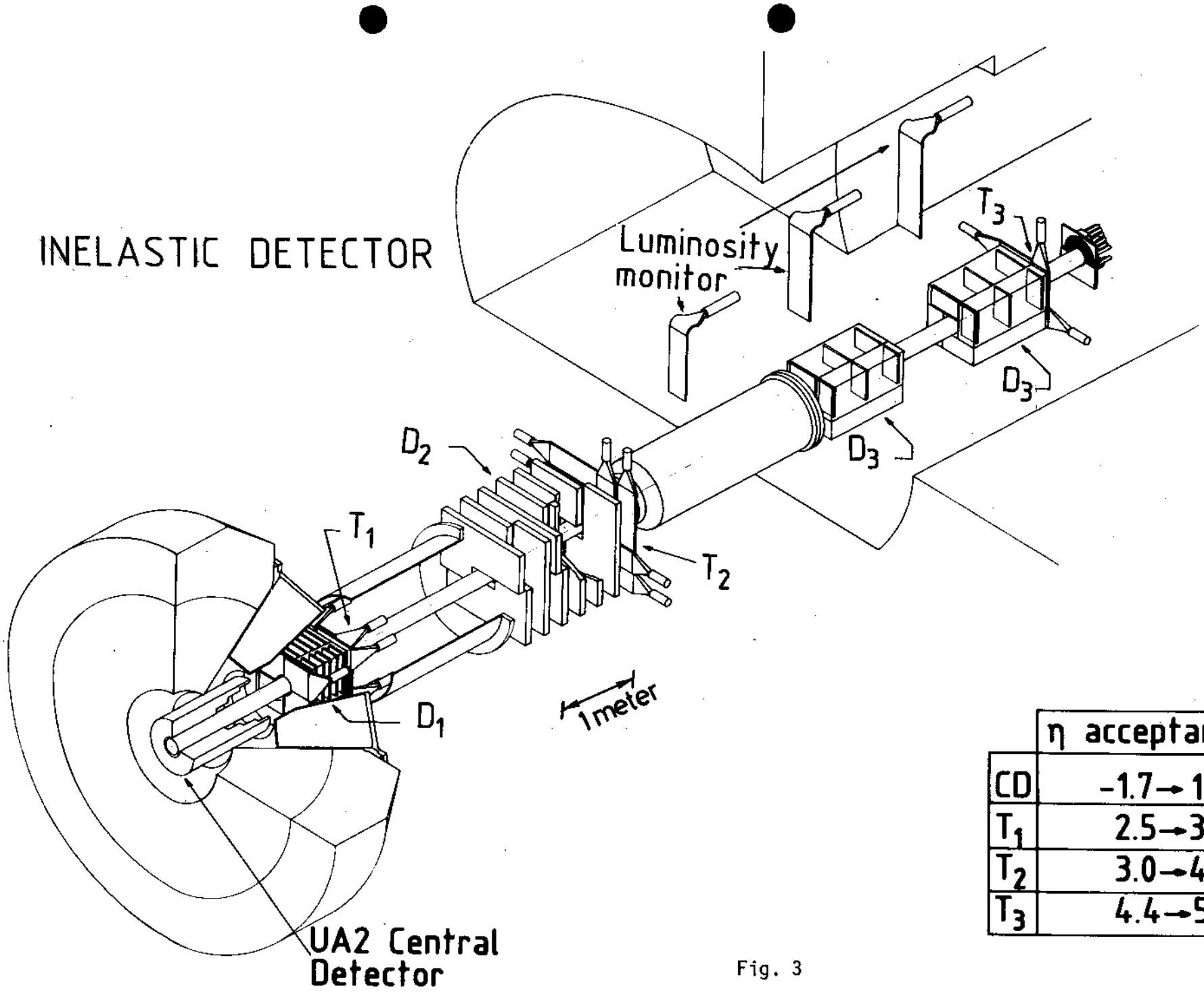

	η acceptance
CD	-1.7→1.7
T_1	2.5→3.5
T_2	3.0→4.8
T_3	4.4→5.6

Fig. 3

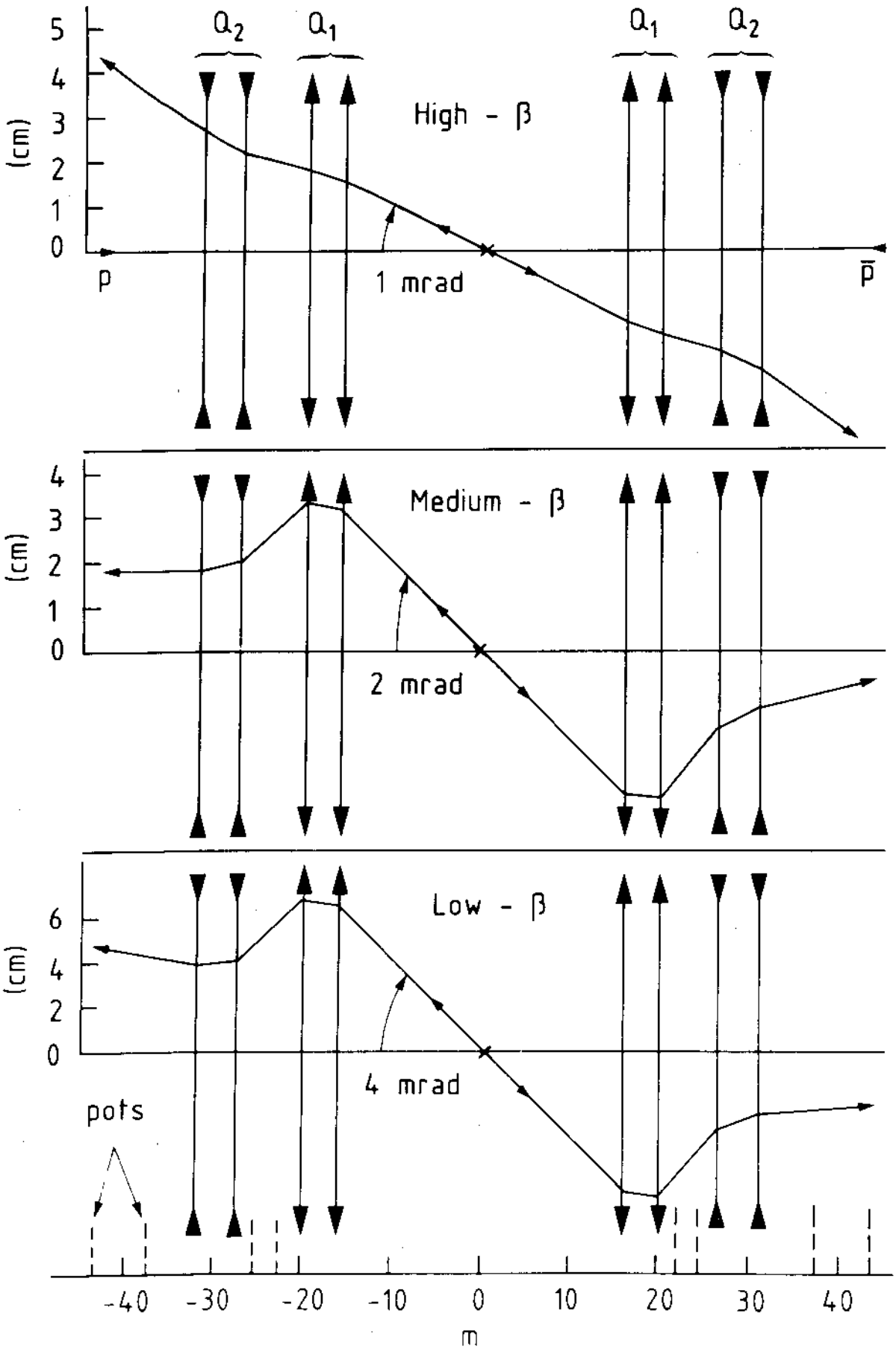
TRAJECTORIES IN THE V-PLANE
Q2
Q1
Q1
Q2
High - β
(cm)
5
4
3
2
1
0
p
1 mrad
p̄
Medium - β
(cm)
4
3
2
1
0
2 mrad
Low - β
(cm)
6
4
2
0
4 mrad
pots
-40
-30
-20
-10
0
10
20
30
40
m

Fig. 4

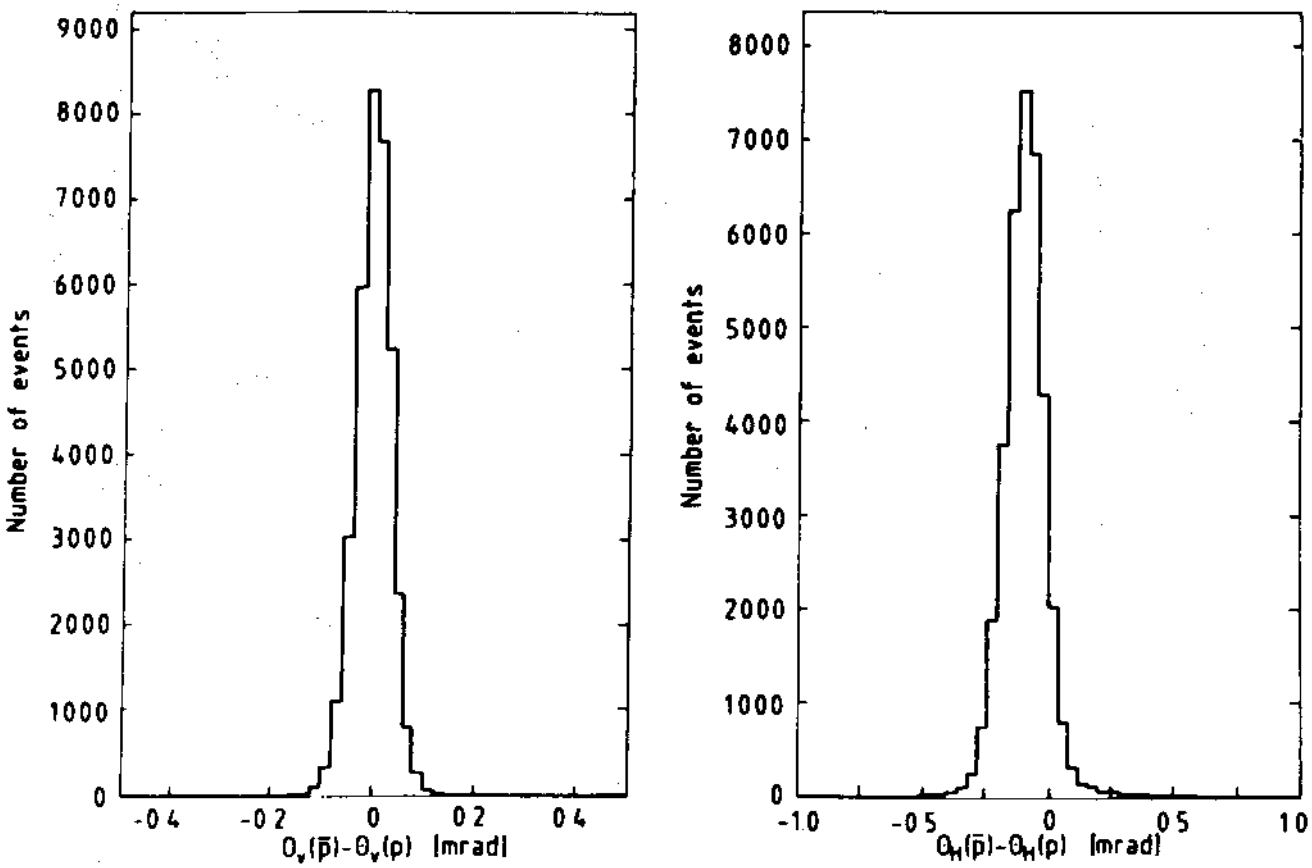
Number of events
9000
8000
7000
6000
5000
4000
3000
2000
1000
0
-0 4
-0 2
0
0 2
0 4
$\theta_v(\bar{p})-\theta_v(p)$ [mrad]
Number of events
8000
7000
6000
5000
4000
3000
2000
1000
0
-1.0
-0 5
0
0 5
1 0
$\theta_H(\bar{p})-\theta_H(p)$ [mrad]

Fig. 5

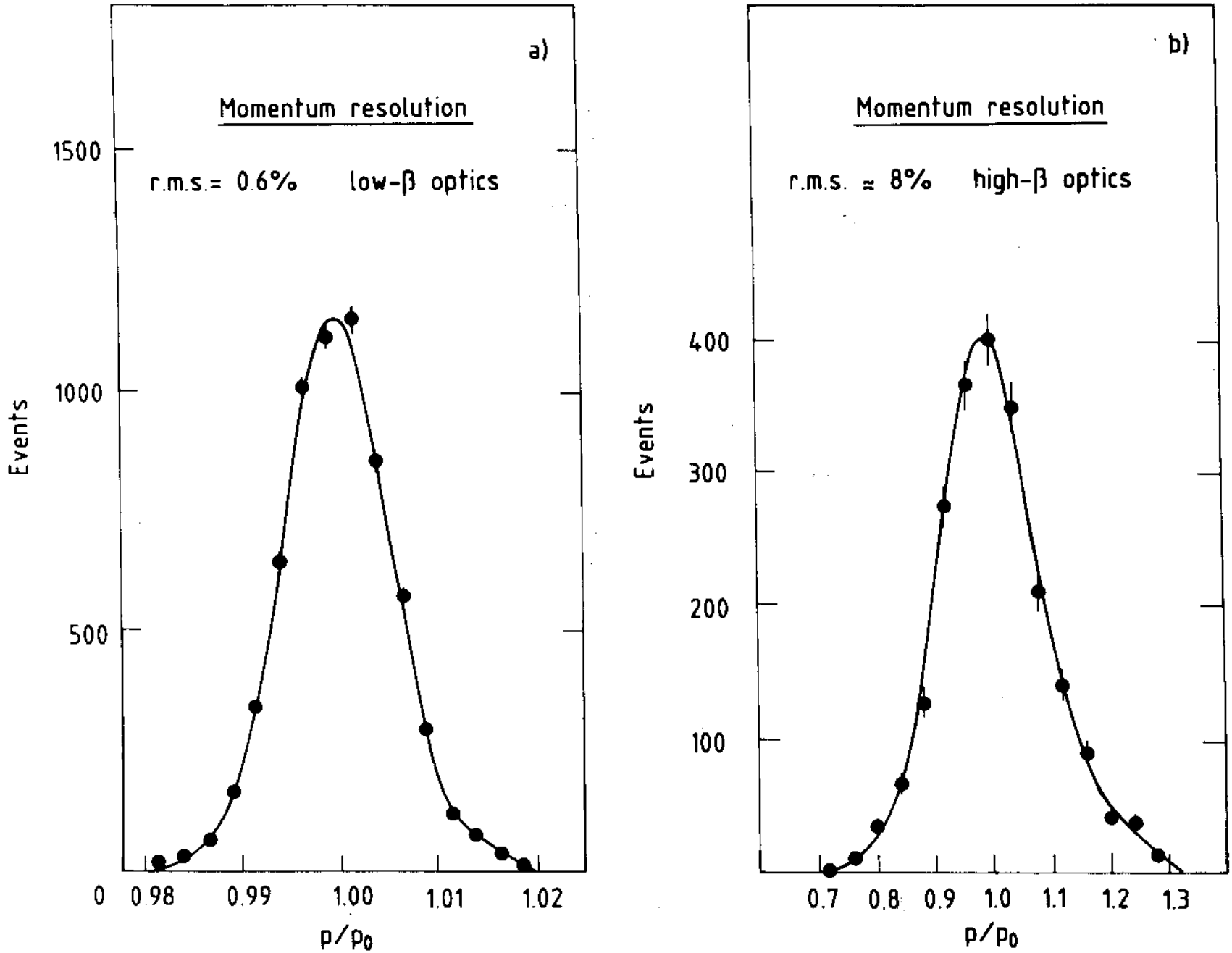
a)
Momentum resolution
r.m.s.= 0.6%
low-β optics
Events
1500
1000
500
0
0.98
0.99
1.00
1.01
1.02
p/p0
b)
Momentum resolution
r.m.s. ≈ 8%
high-β optics
Events
400
300
200
100
0.7
0.8
0.9
1.0
1.1
1.2
1.3
p/p0

Fig. 6

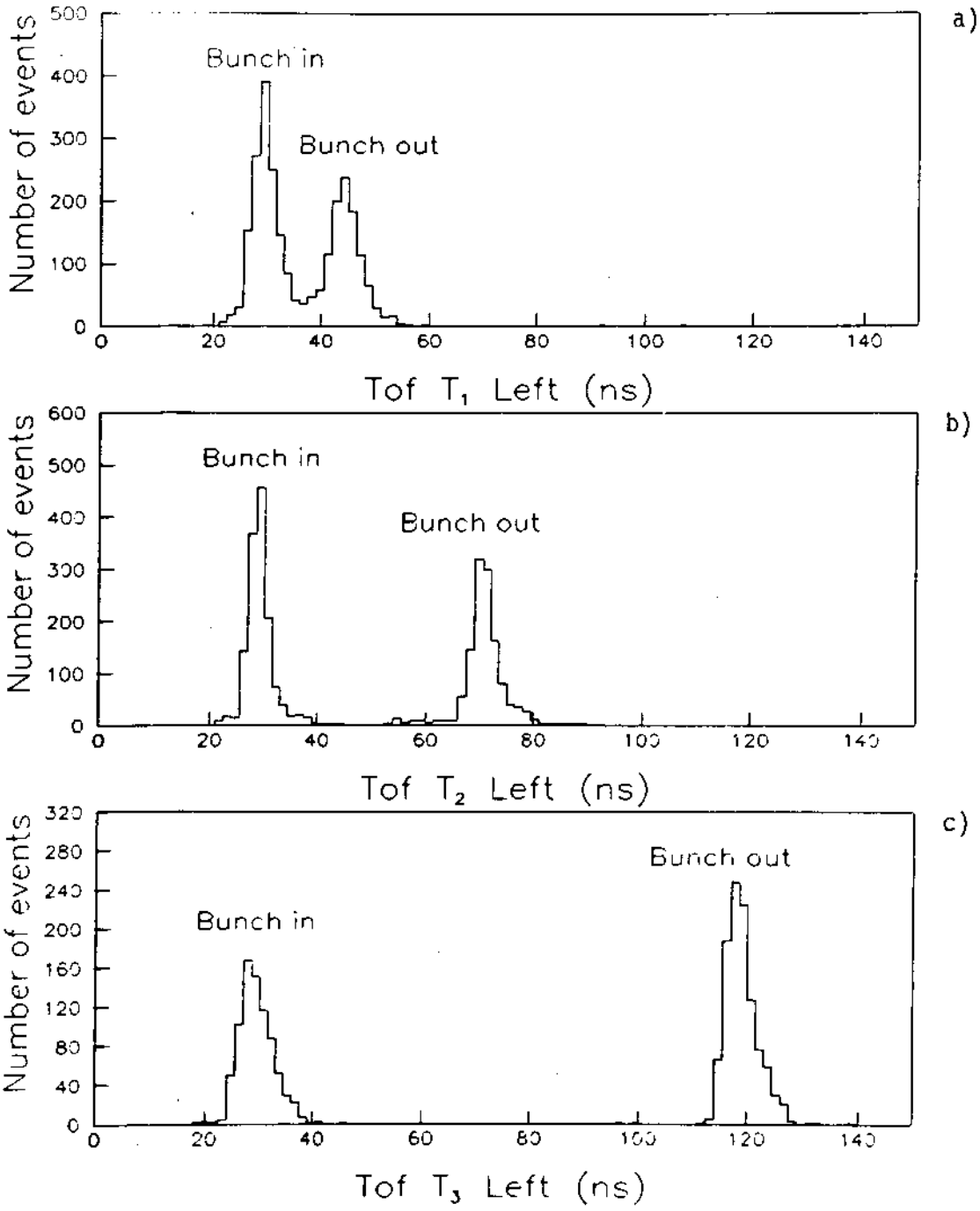
a)
Number of events
Bunch in
Bunch out
Tof T_1 Left (ns)
b)
Number of events
Bunch in
Bunch out
Tof T_2 Left (ns)
c)
Number of events
Bunch in
Bunch out
Tof T_3 Left (ns)

Fig. 7

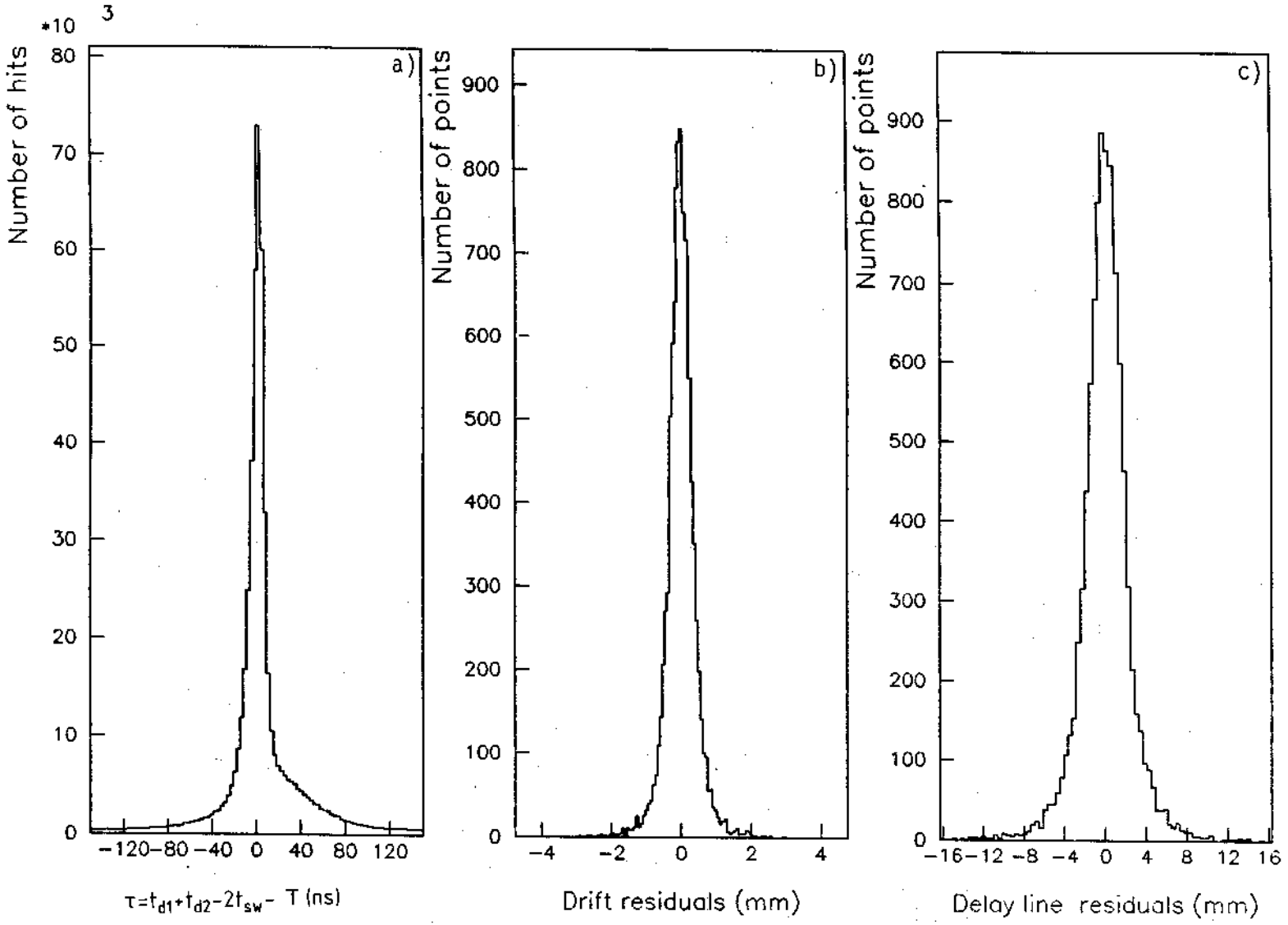
*10 3
Number of hits
a)
τ=t_d1+t_d2-2t_sw- T (ns)
Number of points
b)
Drift residuals (mm)
Number of points
c)
Delay line residuals (mm)

Fig. 8

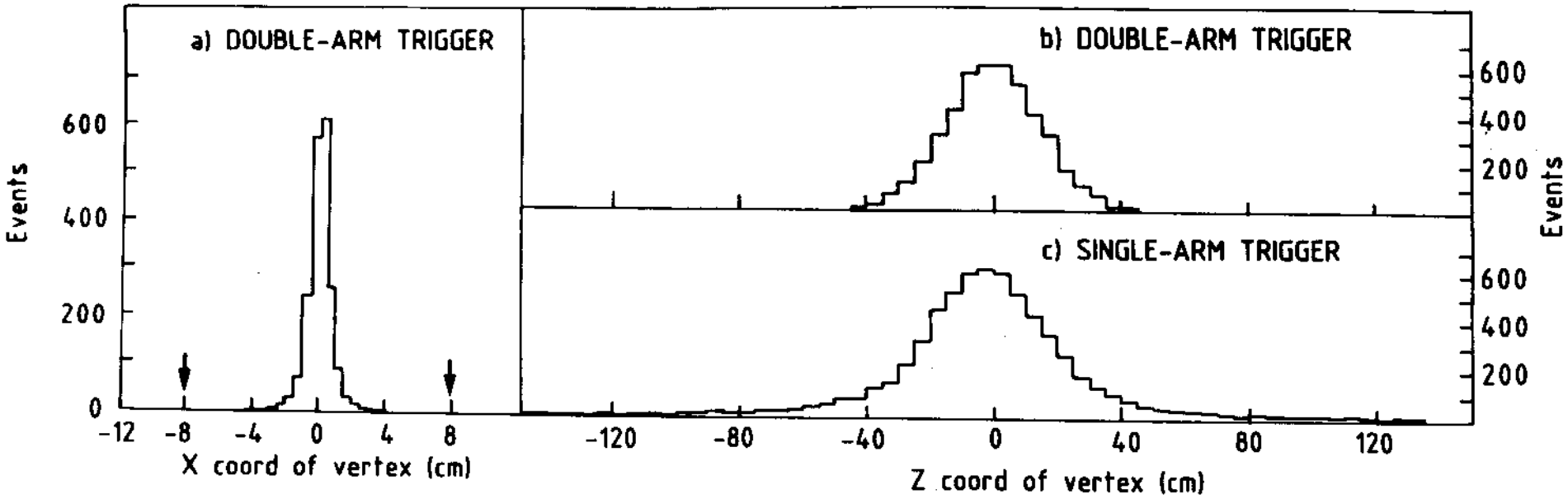
a) DOUBLE-ARM TRIGGER
b) DOUBLE-ARM TRIGGER
c) SINGLE-ARM TRIGGER
Events
600
400
200
0
-12
-8
-4
0
4
8
X coord of vertex (cm)
-120
-80
-40
0
40
80
120
Z coord of vertex (cm)

Fig. 9